Modulation of optical properties with multilayer thickness in antimonene and indiene

Matko Mužević[1], Maja Varga Pajtler[1], Sanjeev Kumar Gupta[2], Igor Lukačević[1]*

[1]*Department of Physics, Josip Juraj Strossmayer University of Osijek, Trg Ljudevita Gaja 6, Osijek, 31000, Croatia*
[2]*Department of Physics and Electronics, St. Xavier's College, Ahmedabad, 380009, India*

*Corresponding author: Tel: (+385) 31232713; E-mail: ilukacevic@fizika.unios.hr

DOI: 10.5185/amlett.2019.2220
www.vbripress.com/aml

Abstract

Optical properties of 2D materials can be effectively modulated by employing multilayer structures with different number of layers. Using the theoretical approach based on density functional theory we simulated relevant optical spectra of antimony and indium mono- and multilayers. We showed that the electronic band structures of antimonene and indiene possess numerous tracking bands enhancing the transition probability. Therefore, high absorption coefficients are found. Modelled multilayer nanostructures of antimonene and indiene experience a red-shift of absorption bands. Antimonene exhibits an optical directional anisotropy regarding the absorbance coefficient and reflectance spectrum for different nanolayer thicknesses. Indiene possesses very high reflectance and refractive index in the visible and IR spectrum which can be effectively modulated by the number of layers. Our work shows that antimonene and indiene multilayers harbour untapped potential for the optical applications at the nanoscale.

Keywords: 2D materials, antimony, indium, optical properties, density functional theory.

Introduction

Following the example of graphene, various two-dimensional materials have entered the stage of nanomaterials. They represent a class of materials which have numerous beneficial properties, like relatively simple morphology, flexibility and easily tunable electronic properties [**1**]. A most natural source of two-dimensional materials is layered bulk materials, such as graphite or phosphorus. Besides them, two-dimensional manifestations were also found for non-layered bulk materials, such as boron, silicon or germanium. That search is still not over and a lot of scientific effort goes into finding new nanomaterials with one-atom thickness.

With intent to use their nano-scale dimensions, researchers are continuously increasing the number of possible applications. Unquestionably an important place among them are optical properties [**2**]. Combined with their advantageous morphological properties, applications in optics establish new opportunities for both research and industry.

Although it may seem at first sight that one-atom-thick material cannot have 'a lot of' interaction with light, exfoliating or synthesizing multilayer 2D materials offers one of the ways to 'enhance' this interaction [**3**]. This can happen either through the modulation of the size of electronic band gap (and consequentially the optical band gap) or direct-to-indirect semiconductor transition (and vice versa) or simply by enlarging the number of atomic layers which consecutively interact with the light.

Among the two-dimensional family of materials, antimony and indium monolayers have drawn a considerable attention [**4-7**]. It has been shown that antimony and indium monolayers, namely, antimonene and indiene, cover different parts of the electromagnetic spectrum. Antimonene has more activity in the ultraviolet part [**8**], while indiene shows more activity in the infrared part of the spectrum [**9**]. They show promising reflective and absorptive properties, albeit in narrow spectral windows. Therefore, it would be relevant and interesting to model their optical activity with respect to the number of layers. Our hypothesis is that their optical properties can be modulated by increasing the thickness of the multilayer. Proving this hypothesis could lead to the improvement in their optical properties and broadening the scope of possible applications in the field of nano-optics.

Theoretical

First-principles calculations were performed based on the density functional theory (DFT) [**10, 11**]. For the theoretical simulations we used the Quantum Espresso code which solves Kohn-Sham equations in a plane-

wave basis set [**12**]. The exchange-correlation functional was approximated within the generalized gradient approximation in the Perdew, Burke, and Ernzerhof parametrization for the calculations of geometries and band structures [**13**]. To calculate the optical properties, we include random phase approximation [**14**]. Only interband transitions were taken into account. The complex dielectric functions were calculated in the energy interval from 0 to 10 eV. More details on obtaining the optical spectra can be found elsewhere [**8**]. Plane-wave energy cutoff was set to 60 and 70 eV for Sb and In, respectively. To study two-dimensional systems under periodic boundary conditions, a vacuum layer with a thickness of at least 16 Å was used to minimize interaction between the neighboring layers. Van der Waals forces were employed to effectively include long-range interactions between the sublayers [**15**]. Monkhorst-Pack k-point meshes of 10×10×1 and 14×14×1 for Sb and In, respectively, were used to approximate the integration over the first Brillouin zone during geometry optimizations of monolayer [**16**]. All atoms and crystal unit cells have been fully relaxed until residual forces and stresses were converged to 0.05 eV/Å and 0.5 kbar, respectively. Total energy convergence criterion was 10^{-3} eV/atom.

Results and discussion

Antimonene was predicted theoretically to be stable in the buckled and puckered geometries with similar cohesive energies [**17**]. However, only the buckled form was realized experimentally [**18**]. A lattice constant of 4.13 Å was measured using STM and a buckling height of 1.65 Å was predicted based on a model. Out theoretical data agree almost perfectly with these experimental results (**Table 1**). Indiene has been so far only predicted theoretically [**19**]. It was predicted to be stable in its planar and buckled geometries. Its planar form, however, has two very soft acoustic phonon modes. Because of this fact, and to synergize the comparison with the case of antimonene, we will consider only the buckled indiene. If one compares their geometries (**Fig. 1a** and **Fig. 1b**), it is visible that antimonene has a larger lattice constant, but a much smaller buckling height. Thus, during the relaxation indiene narrows its bond angles, which leads to larger bond lengths. These structural characteristics are related to the bonding properties, which can be illuminated by the electron density (**Fig. 1c** and **Fig. 1d**). It is clearly seen that in indiene there is a much stronger localization of electron density around the atomic centers, while simultaneously there is no density along the bonds. Relatively stronger bonding is found in antimonene, which leads to shorter buckling heights. Localized electron density in antimonene corresponds to the ELF picture obtained by Wu *et al.* [**18**].

Upon addition of more layers, distinctive difference is observed between antimonene and indiene (**Fig. 1a** and **Fig. 1b**). Second layer of buckled antimonene separates itself from the first one by 2.30 Å (**Table 1**). This is much larger than an intralayer distance (or buckling height) of 1.63 Å, which doesn't change with respect to the monolayer case. Same trend is preserved upon addition of a third layer. Electron density, again, explains this difference. Between the layers there is negligible density, giving no electron bonding (**Supp. Fig. 1a**). As our simulations included van der Waals interaction, this speaks of the relevance of long-range forces in multilayer 2D systems. On contrary, in indiene the interlayer distance is about the same as the intralayer distance (**Table 1**) in both bi- and trilayer cases. Weak bonding between the sublayers and between the layers points to the equal separation. It is possible that a single buckled monolayer of indiene can be actually understood as two planar monolayers with strong ionic bonding inside and between the planes (**Supp. Fig. 1b**).

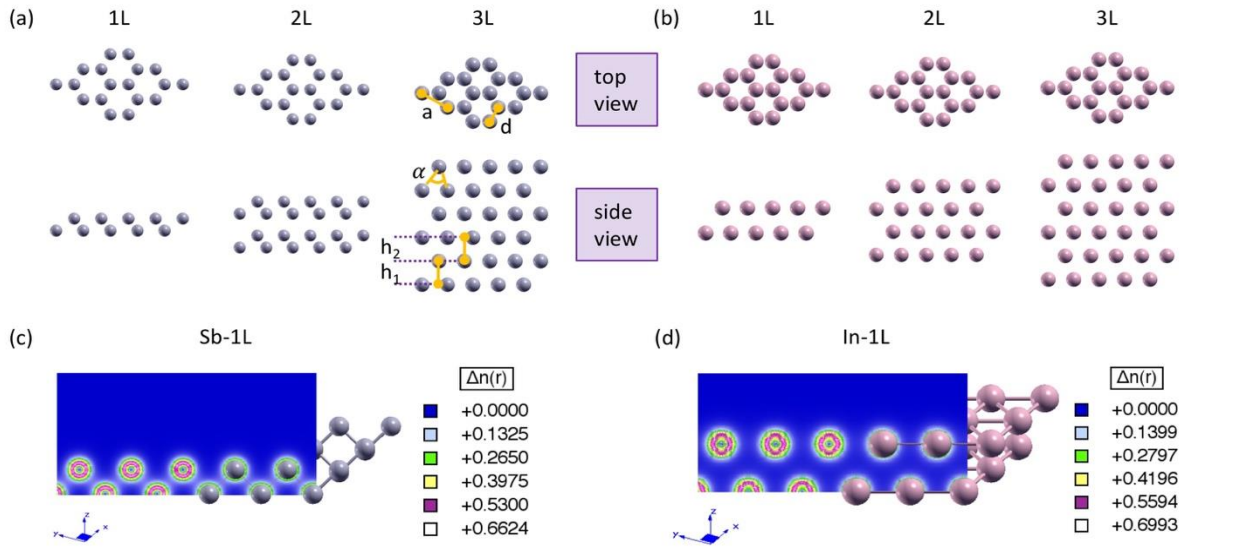

Fig. 1. (a)/(b) Top and side views of mono- and multilayer buckled antimonene/indiene. Yellow lines indicate the distances and angles as given in Table 1. All structures relax to the lowest energy configuration with AA stacking. (c) Electron charge density in monolayer antimonene in the plane along the bond. (d) Electron charge density in monolayer indiene in the plane along the bond.

Table 1. Structural data of mono- and multilayer antimonene (buckled) and indiene (buckled and planar): lattice constant (a), bond length (d), intralayer distance (h_1), interlayer distance (h_2) and interlayer bond angle (α).

		a (Å)	d (Å)	h_1 (Å)	h_2 (Å)	α (°)
Sb buckled	1L	4.13	2.89	1.63		91.23
	2L	4.07	2.90	1.63	2.30	91.75
	3L	4.08	2.88	1.65	3.00	90.36
In buckled	1L	3.23	3.43	2.88		56.16
	2L	3.39	3.41	2.79	2.75	59.58
	3L	3.38	3.41	2.80	2.79	59.32

The origin of optical properties can be found in the electronic band structure of a material. Thus, we first calculated the electronic band structure of antimonene and indiene along high-symmetry directions in the Brillouin zone (**Fig. 2**). More or less flat bands in antimonene and a multitude of tracking bands in indiene promise a lot of optical activity for these two materials. These features are retained in bi- and trilayer antimonene and indiene. With addition of new electronic bands with similar characteristics in multilayer structures, we can expect the appearance of a multitude of optical bands.

The influence of adding more layers to the antimonene and indiene is best seen in the optical characteristics shown in **Fig. 3**. Absorption coefficient, A, generally increases with the increase of nanolayer thickness, i.e. the number of layers, which is expected. Three more effects can be observed: (i) in antimonene a clear shift of the absorption edge is visible due to the lowering of the band gap, (ii) more absorption bands appear in bi- and trilayer nanostructures due to the increased number of electronic bands and consequently the number of transitions, and (iii) for the light

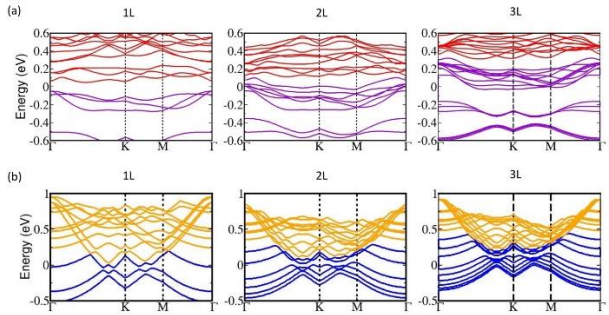

Fig. 2. (a) Electronic band structure mono- and multilayer buckled antimonene. In 2L and 3L multilayers antimonene makes a transition from indirect semiconductor to semimetal. (b) Electronic band structure mono- and multilayer buckled indiene. In 3L multilayer indiene makes a transition from semimetal to metal.

polarization perpendicular to the layers ('zz'-components), the absorption bands are shifted toward the smaller energies. These shifts correspond to the relative energy changes of the electronic bands. The corresponding bands cannot be easily identified because of the complexity of the band structures. In antimonene, UV absorption band around 5 eV red-shifts by 0.83 eV upon mono- to bilayer change, and by 0.37 eV upon bi- to trilayer change (**Fig. 4a**). For about the same increase in nanolayer thickness, visible absorption band in indiene experiences smaller shifts: 0.54 eV (mono- to bilayer change) and 0.14 eV (bi- to trilayer change). The origin of this difference could be sought for in lesser shift of electronic bands in indiene than in antimonene. Largest absorption coefficient is found for monolayer indiene. While for indiene its position is in the long-wavelength visible or infra-red spectrum, in antimonene it is in UV. This agrees with the optical measurements on few-layer antimonene [**20**]. However, in indiene it drops fast in multilayer form. In trilayer

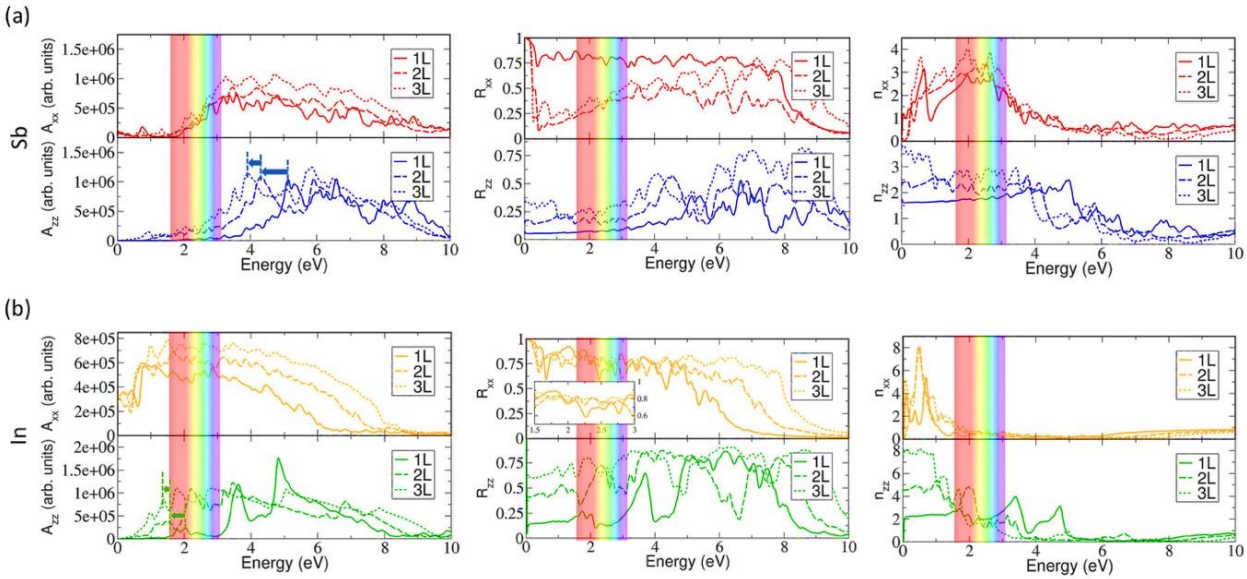

Fig. 3. (a) Absorption coefficient, A, reflectance spectra, R, and refractive index, n, of 1L, 2L and 3L antimonene. (b) Absorption coefficient, A, reflectance spectra, R, and refractive index, n, of 1L, 2L and 3L indiene. Two components are shown for each optical property: 'xx'-component for the light polarization parallel to the monolayer plane, and 'zz'-component for the light polarization perpendicular to the monolayer plane. Block-arrows indicate peak shifts due to the increase of layer thickness. Inset in R_{xx} spectrum of indiene shows reflectance around the visible part of the electromagnetic spectrum.

structure antimonene has the largest absorption coefficient (**Fig. 4b**). This decrease of absorption maximum happens only for A_{zz} in indiene. Other absorption coefficients experience an increase with the increase of number of layers. This kind of optical anisotropy could be useful in optical devices which would combine mono- and multilayer indiene. Through comparison with graphene and MoS_2, two-dimensional materials which have been extensively studied, we see that indiene and antimonene have about the same absorption quality as MoS_2, while outperforming graphene: $A_{MoS2} = 1\text{-}1.5\times10^6$, $A_{graphene} = 0.7\times10^6$, $A_{indiene} = 1.7\times10^6$, $A_{antimonene} = 1\times10^6$.[16] Increase in the absorption coefficient with the number of layers is almost linear. The same behavior is seen also in MoS_2 [**21**].

Reflectance of the visible light behaves differently in multilayer antimonene and indiene (**Fig. 3**). While in indiene there are no significant changes, in antimonene reflectance for the light polarized parallel to the nanolayer plane drops by about 50% (**Fig. 4c**). For the visible light polarization perpendicular to the monolayer plane, the effect of adding more layers is the same: it increases, albeit differently. In multilayer indiene, the increase is threefold and reaches over 80% (**Fig. 4c**). High reflectance in indiene could find its applications in ultrathin flexible reflectors. The variations in reflectance spectrum tend to stabilize themselves, meaning that indiene could also play a role of wide-band reflector from IR to UV part of the electromagnetic spectrum. Conversely, reflectance in antimonene increases slowly with the photon energy, but does not reach significant values until deep UV, which could be useful for UV mirrors.

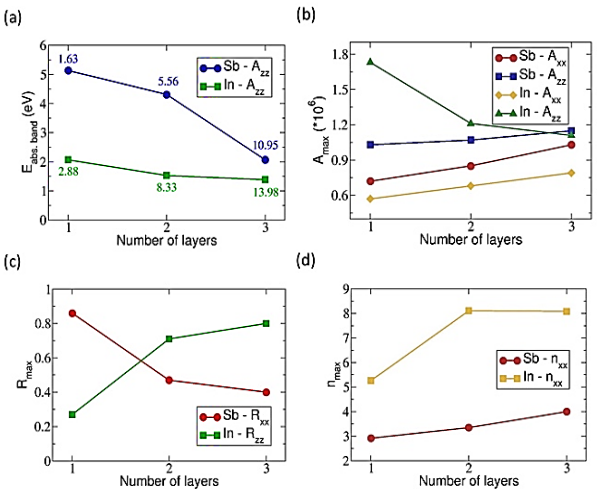

Fig. 4. (a) Positions of absorption bands in buckled antimonene and indiene. Both bands are red-shifted toward lower energies. Numbers besides the positions denote the nanolayer thickness for the corresponding number of layers. (b) Absorption coefficient maxima of buckled antimonene and indiene and their dependence on the number of layers. (c), (d) Dependence of reflectance/refractive index maxima on the number of layers in buckled antimonene and indiene.

Refractive index is an important optical quantity, as it gives information on how the impending light behaves once it enters the material. For the visible light antimonene will have more influence than indiene, as its refractive index increases from to 4 (**Fig. 4d**). Indiene, however, exhibits its influence in the IR part of the spectrum. There its refractive index reaches 8. This value greatly surpasses even the ones of the most studied transition metal chalcogenides [**22**]. Thus, we could place indiene as an extremely high refractive material for the IR light applications.

Conclusion

Using *ab initio* simulations, we showed that antimony and indium mono- and multilayer structures possess noticeable optical properties. These optical properties are predicted to be effectively modulated by additional layers. Their electronic band structures with numerous tracking bands allow a myriad of optical transitions with high transition probability. Consequently, we found high absorption coefficients in both antimonene and indiene compared to monoelemental monolayers with similar structures. Further work should be concentrated on redefining the absorption related properties for two-dimensional materials, so that they can be compared to the ones of bulk materials. More interesting optical properties are antimonene's and indiene's reflectance and refractive index. Reflectance over 80% in indiene can be compared to those of commercial reflective materials, like rutile. However, it peaks in IR spectrum and it is not constant enough to be yet considered for real applications. It does present a lot of potential taking into account that reflectance can be further modified using various techniques, like doping or surface functionalization. These are the subjects of future studies. Refractive index of antimonene can be compared to the ones of transition metal chalcogenides. On the other hand, refractive index of indiene surpasses even those. However, the refractive index maximum is localized in a very narrow energy segment and placed in the IR part of the spectrum. Finding a way to broaden the refraction maximum and shifting it toward the visible wavelengths will be of utmost importance for the future applications. This high value promises a number of possible applications, such as ultrathin antireflection coatings, light extractors, encapsulants and in prevention of IR light or heat losses.

Acknowledgements

This work was supported by HPC-Europa3 Transnational Access programme. M.M. thanks the HPC-Europa3 visitor programme.

Author's contributions

Conceived the plan: IL, SKG; Performed the calculations: MM; Data analysis: MVP; Wrote the paper: IL, SKG. Authors have no competing financial interests.

Supporting information

Supporting informations are available from VBRI Press.

References

1. Xu, R.; Zou, X.; Liu, B.; Cheng, H. M., *Materials Today*, **2018**, *21*, 391.
2. Zhou, X.; Hu, X.; Yu, J.; Liu, Sh.; Shu, Zh.; Zhang, Q.; Li, H.; Ma, Y.; Xu, H.; Zhai, T., *Adv. Funct. Mater.*, **2018**, *28*, 170658.
3. Bernardi, M.; Ataca C.; Palummo M.; Grossman J. C., *Nanophotonics*, **2017**, *6*, 479.
4. Shao Y. et al.; *Nano Lett.*, **2018**, *18*, 2133.
5. Wang, X.; Song, J.; Qu, J., *Angewandte Chemie*, **2018**. **DOI:** 10.1002/anie.201808302.
6. Ares, P.; Palacios, J. J.; Abellán, G.; Gómez-Herrero, J.; Zamora, F., *Adv. Mater.*, **2018**, *30*, 1703771.
7. Kripalani, D. R.; Kistanov, A. A.; Cai, Y.; Xue, M.; Zhou, K., *Phys. Rev. B*, **2018**, *98*, 085410.
8. Singh, D.; Gupta, S. K.; Sonvane, Y.; Lukačević, I., *J. Mater. Chem. C*, **2016**, *4*, 6386.
9. Optical Properties of 2D Indium Allotropes, Singh, D.; Gupta, S. K.; Lukačević, I.; Mužević, M.; Sonvane, Y., in progress.
10. Hohenberg, P.; Kohn, W., *Phys. Rev.*, **1964**, *136*, B864.
11. Kohn, W.; Sham, L. J., *Phys. Rev.*, **1965**, *140*, A1133.
12. Giannozzi, P.; Baroni, S.; Bonini, N.; Calandra, M.; Car, R.; Cavazzoni, C.; Ceresoli, D.; Chiarotti, G. L.; Cococcioni, M.; Dabo, I.; Dal Corso, A.; Fabris, S.; Fratesi, G.; de Gironcoli, S.; Gebauer, R.; Gerstmann, U.; Gougoussis, C.; Kokalj, A.; Lazzeri, M.; Martin-Samos, L.; Marzari, N.; Mauri, F.; Mazzarello, R.; Paolini, S.; Pasquarello, A.; Paulatto, L.; Sbraccia, C.; Scandolo, S.; Sclauzero, G.; Seitsonen, A. P.; Smogunov, A.; Umari, P.; Wentzcovitch, R. M., *J. Phys.: Condens. Matter.*, **2009**, *21*, 395502.
13. Perdew, J. P.; Burke, K.; Ernzerhof, M., *Phys. Rev. Lett.*, **1997**, *77*, 3865.
14. Gajdoš, M.; Hummer, K.; Kresse, K.; Furthmüller, J.; Bechstedt, F., *Phys. Rev. B*, **2006**, *73*, 045112.
15. Grimme, S., *J. Comp. Chem.*, **2006**, *27*, 1787.
16. Monkhorst, H. J.; Pack, J. D., *Phys. Rev. B*, **1976**, *13*, 5188.
17. Wang, G.; Pandey, R.; Karna, Sh. P., *ACS Appl. Mater. Interfaces*, **2015**, *7*, 11490.
18. Wu, X.; Shao, Y.; Liu, H.; Feng, Z.; Wang, Y. L.; Sun, J. T.; Liu, C.; Wang, J. O.; Liu, Z. L.; Zhu, S. Y.; Wang, Y. Q.; Du, S. X.; Shi, Y. G.; Ibrahim, K.; Gao, H. J., *Adv. Mater.*, **2017**, *29*, 1605407.
19. Singh, D.; Gupta, S. K.; Lukačević, I.; Sonvane, Y., *RSC Adv.*, **2016**, *6*, 8006.
20. Ares, P.; Zamora, F.; Gomez-Herrero, J., *ACS Photonics*, **2017**, *4*, 600.
21. Bernardi, M.; Palummo, M.; Grossman, J. C., *Nano Lett.*, **2013**, *13*, 3664.
22. Liu, H. L.; Shen, Ch. Ch.; Su, Sh. H.; Hsu, Ch. L.; Li, M. Y.; Li, L. J., *Appl. Phys. Lett.*, **2014**, *105*, 201905.

